GeoNeurale

Diffractions, reflections, Vp and Vs - Part 1

In this article we describe different theories concerning wave propagation related to migration and velocity analysis methods and in part 2 we will derive some considerations by resuming these theories. We start a discussion and we welcome feedback and contributions.

CIG

Quality control on common offset gathers domain has always been an important phase of the seismic processing workflow. Since many years regarded as a method of continuous reflector exploration and imaging, the concept related to common image gathers (CIG) can be illustrated in the 3D prestack volume for 2D seismic data and 4D prestack volume for 3D seismic data or even 5D when azimuthal shot-receiver directions are taken into consideration for reservoir anisotropy studies and increasing fold and S/N ratio. Sorting this data volume is used in the Prestack time migration and Prestack depth migration with tomographic velocity model building although a strictly physical approach and efficient variant for migration algorithms could be a sorting volume in the common scattering angle domain.

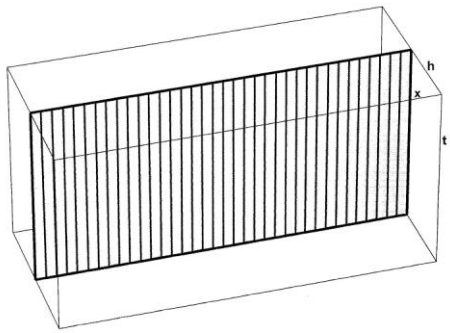

Fig. 1 schematic representation of prestack volume on 2D seismic .
Constructing common offset gathers with a constant offset h of the x-t gather. Cy: J.C. Bancroft

The goal is to follow reflector imaging continuity in terms of semblance and amplitude attributes (track the image of the reflector point).
Then CMP and AVO data sorting itself can be then implemented as a subdomain of these volumes.

In the CMP Kirchhof summation theory we model the effect of a reflection element as a diffractor point, where the amplitudes are summed along the diffraction hyperbola, taking into account and equalizing for difference in normal moveout (higher for diffractions than for reflections Fig. 2).

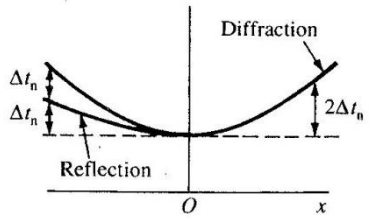

Fig. 2 Difference in NMO between Reflection and Refraction as CDP gather representation Cy.: R.E. Sheriff

In the commom offset domain only the zero offset apex is coincident with the scatter point, increasing the offset will lower the apex of the hyperbola with respect to the scatter point.

Diffractions appear when the wavelength of the incident wave has comparable dimension of the curvature ray of the diffracting element. It can identify fault edges but also geological bodies of different density / wave velocity from the surrounding formation.
CIG offer the opportunity to study the be behavior of diffracting elements as a function of the diffraction angle. In homogeneous isotropic environment diffractions would be represented by simmetrical Cheops pyramid in (Fig. 3).

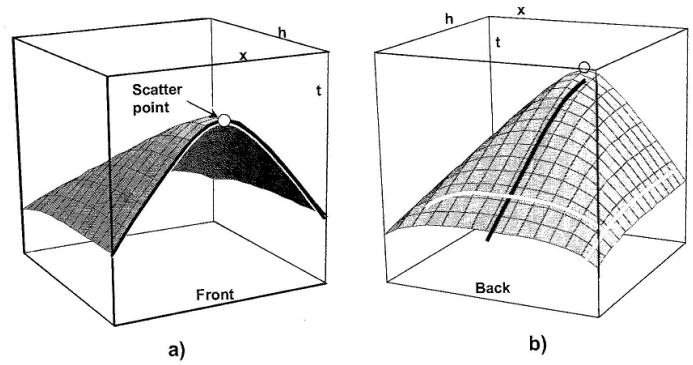

Fig. 3 Simple Cheops pyramid structure as envelope of discrete offset (h) for 2D seismic.
a. Scatter point in the zero-offset section (CMP section),
b. Increasing constant offset increases distance of hyperbolas apex from scatter point. Cy: J.C. Bancroft

The physical reality is that diffraction wavefields which normally detect reflectors discontinuity can be present anywhere but often the amplitude is too law to be detected by receivers.
Expecially in carbonate formations, diffractors are important features to interpret inter-formational heterogeneity, in clastic formations these elements can delineate depositional heterogeneity within the same lithological formation.

Any discontinuity in density and velocity even within the same formation with curvature/ dimension smaller of the wavelength can cause diffractions.

A DIFFRACTION THEORY

An old model (E. Savarensky) describes a diffracting element excited by an incident wave which emits secondary diffracted waves proportional to its volume and the wave amplitude (in this case a unit volume proportional to unit amplitude). Although the result has to be updated for wave energy and volume of the element, this is a valid alternative representation of the phenomenon geometry.

This can be physically modeled starting from a point source theory of a translational oscillation in the medium. The inverse problem leads to the theory of diffraction sources.

Fig. 4 shows the model of a body source **F** acting on a volume **V** in the **Z** direction, producing longitudinal and transverse wave of amplitude $\mathbf{U}r$, $\mathbf{U}_\theta$ on the measurement point **M** at a great distance **R** apart

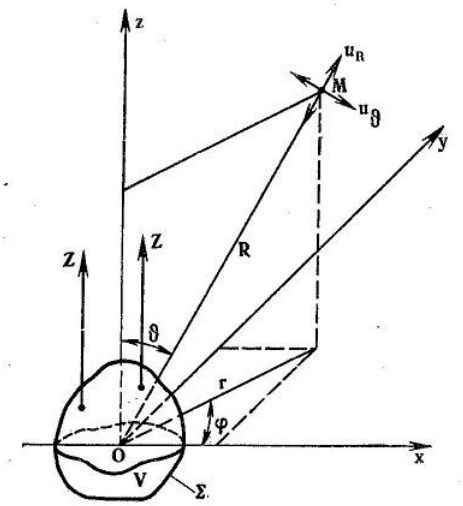

Fig. 4 Model of a body source **F** acting on a volume **V** and reciprocal source of P and S waves
Cy. : E. Savarensky

The initial condition of elastic wave displacement at the source **U**, caused by the force **F**, with velocity of propagation **a** for longitudinal waves and **b** for transversal waves is:

$$a^2\nabla^2 \operatorname{div} \mathbf{U} + \operatorname{div} \mathbf{F} = \frac{\partial^2 \operatorname{div} \mathbf{U}}{\partial t^2}$$

$$b^2\nabla^2 \operatorname{curl} \mathbf{U} + \operatorname{curl} \mathbf{F} = \frac{\partial^2 \operatorname{curl} \mathbf{U}}{\partial t^2}$$

Eq. 1

If the force is variable on time as a harmonic oscillation, the elastic conditions applied to the force, for displacement **dz** in the **Z** direction, with angular frequency ω are:

$$\operatorname{div} \mathbf{F} = \frac{\partial Z}{\partial z} e^{i\omega t}, \quad \operatorname{curl}_x \mathbf{F} = \frac{\partial Z}{\partial y} e^{i\omega t}$$

$$\operatorname{curl}_y \mathbf{F} = -\frac{\partial Z}{\partial x} e^{i\omega t}, \quad \operatorname{curl}_z \mathbf{F} = 0$$

Eq.2

these can be substituted in eq. 1 .

The solution on the integral equations on the volume **V** for great distances **R** give the wave equations for longitudinal and transversal waves $\mathbf{u_r}$, $\mathbf{u_\theta}$:

$$u_R = \frac{ZV}{4\pi a^2 R} e^{i\omega\left(t-\frac{R}{a}\right)} \cos\vartheta$$

$$u_\vartheta = -\frac{ZV}{4\pi b^2 R} e^{i\omega\left(t-\frac{R}{b}\right)} \sin\vartheta$$

Eq. 3

Which show as in fig 2 a direct dependence (polarization) as function of the angle θ

Applying this equation for a rigid sphere of Volume 4/3 π l^3
Considering the sphere with density ρ_1 != ρ of the medium oscillating with frequency ω and amplitude ωo :

$$u_R = -\frac{4}{3}\pi\left(\frac{l}{\lambda_a}\right)^2 \frac{w_0\rho_1}{(R/l)\,\rho} \cos\vartheta e^{i\omega\left(t-\frac{R}{a}\right)}$$

$$u_\vartheta = \frac{4}{3}\pi\left(\frac{l}{\lambda_b}\right)^2 \frac{w_0\rho_1}{(R/l)\,\rho} \sin\vartheta e^{i\omega\left(t-\frac{R}{b}\right)}$$

Eq. 4

Therefore the amplitudes depend on ***l*** = radius of the sphere, λ a , λ b respective wavelength of longitudinal and transverse waves,

From this solution it is possible to derive the equations of diffracted waves from a sphere of radius ***l*** when a plane incident longitudinal wave

$$w_0 e^{i\omega(t-z/a)}$$ Eq. 5

strikes the sphere.

If the density of the sphere is different from that of the medium, then the force per unit mass which produces the diffracted waves is:

$$-\frac{(\rho_1-\rho)}{\rho}\,\omega^2 w_0 e^{i\omega t}$$

Eq. 6

The equations obtained for the field of secondary diffracted waves from a spherical inclusion are:

$$u_R = -\frac{4}{3}\pi\left(\frac{l}{\lambda_a}\right)^2 \frac{w_0(\rho_1-\rho)}{(R/l)\,\rho}\cos\vartheta e^{i\omega\left(t-\frac{R}{a}\right)}$$

$$u_\vartheta = \frac{4}{3}\pi\left(\frac{l}{\lambda_b}\right)^2 \frac{w_0(\rho_1-\rho)}{(R/l)\,\rho}\sin\vartheta e^{i\omega\left(t-\frac{R}{b}\right)}$$

Eq. 7

As we see , the amplitudes depend on: l , λ a , λ b , the difference in density and the direction of propagation of the wave give by θ .
The model show that P waves propagate upward and downwards with maximal amplitude parallel to the z axis, S waves propagate laterally with maximal amplitude on the plane x-r.

For the special case of a sphere the model has symmetric planes s-r , x-z, r-z .
This will correspond to a radiation pattern of lobes with symmetry axis z for P waves and symmetry plane x-r for S waves.
The unconcentrated energy distribution compared to theoretical pure reflections form diffraction hyperbolas on the CIGs, the energy smoothly distributed along the hyperbola.
P waves laterally hitting the body will cause S waves propagating laterally with highest intensity.

The common offset measurements sorted in the common image gather CIG will contain both reflections and refractions.
This configuration forms the basis of prestack time migration and prestack depth migration.

SUBSURFACE OFFSET COMMON IMAGE GATHERS

If the CIG offers an optimal instrument for QC applications on surface measurements, systems based on forward and backpropagated wavefields offers a complementary approach to the previous methods for velocity analysis and migration.
To distinguish from surface CIG, subsurface offset common image gathers (SO-CIG) should consider only reflections from maximum reflectivity in the sense of seismic impedance contrast to optimize the calculation of the correlation coefficient between equal time incident and reverse-time-migration wavelets.

This is a wavefield extrapolation method in the angle domain and velocity analysis is based on different methods than surface CIG. The technique is based on correlation at constant time intervals of from the source S forward incident and from the receiver R backpropagated wavefields within a velocity model, starting from the initial ray parameters measured in S and R.
The maximal correlation will identify the reflection point.

Forward and backward propagation are modeled starting at the surface with the direction indicated by the wave parameter **p** and with trajectory calculated with the snell law considering the interval velocities and anisotropy in the model.
Starting at the reflection point upwards a correlation is calculated, the correlation versus time are reportd in fig. 5. The model for a dipping reflector shows correlation at the reflection point but different correlations coefficients away from the X_{CIG} position.

This is a theoretical model showing that the maximal correlation occurs at the reflection point.
The slope of the time correlation function is a function of the reflection angle ψ .
This means the direction (inclination) of the wavefield are related to the correlation function.
Fig. 7 .
(Jeannot et al. , Bruin et al. 1990) (Sava and Fommel 2006), (Rosales, Fomel, Biondi. Sava 2008), (Rickett and Sava 2002).
Fig. 5 shows the correlation function for a specific depth but in the time domain, this concept can be extended at different depths around the reflection point.
Subsurface offset gathers are constructed by displacing the incident and reflected wavefield in opposite directions symmetrically to the Imaging point X_{CIG} of constant offsets h/2 and calculating the correlation of the upgoing and downgoing wavefields at constant times in the X_{CIG} position.

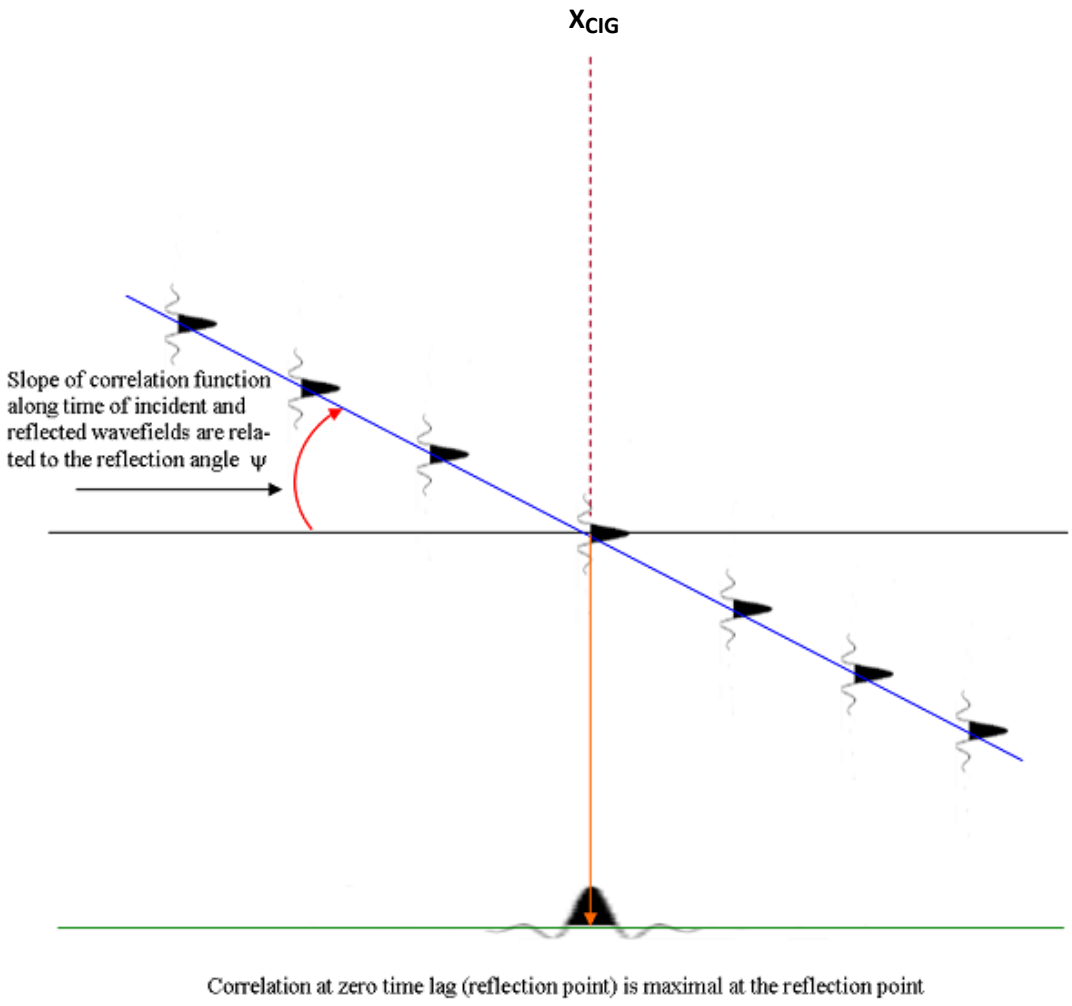

Fig 5. Correlation function for a specific depth in the time domain, the concept can be extended at different depths around the reflection point. Ref. E. Robein 2010

Fig. 6a shows the relationship between forward and backpropagated wavefields in the time domain and the technique to correlate these in time to search the maximal correlation point in time and offset.

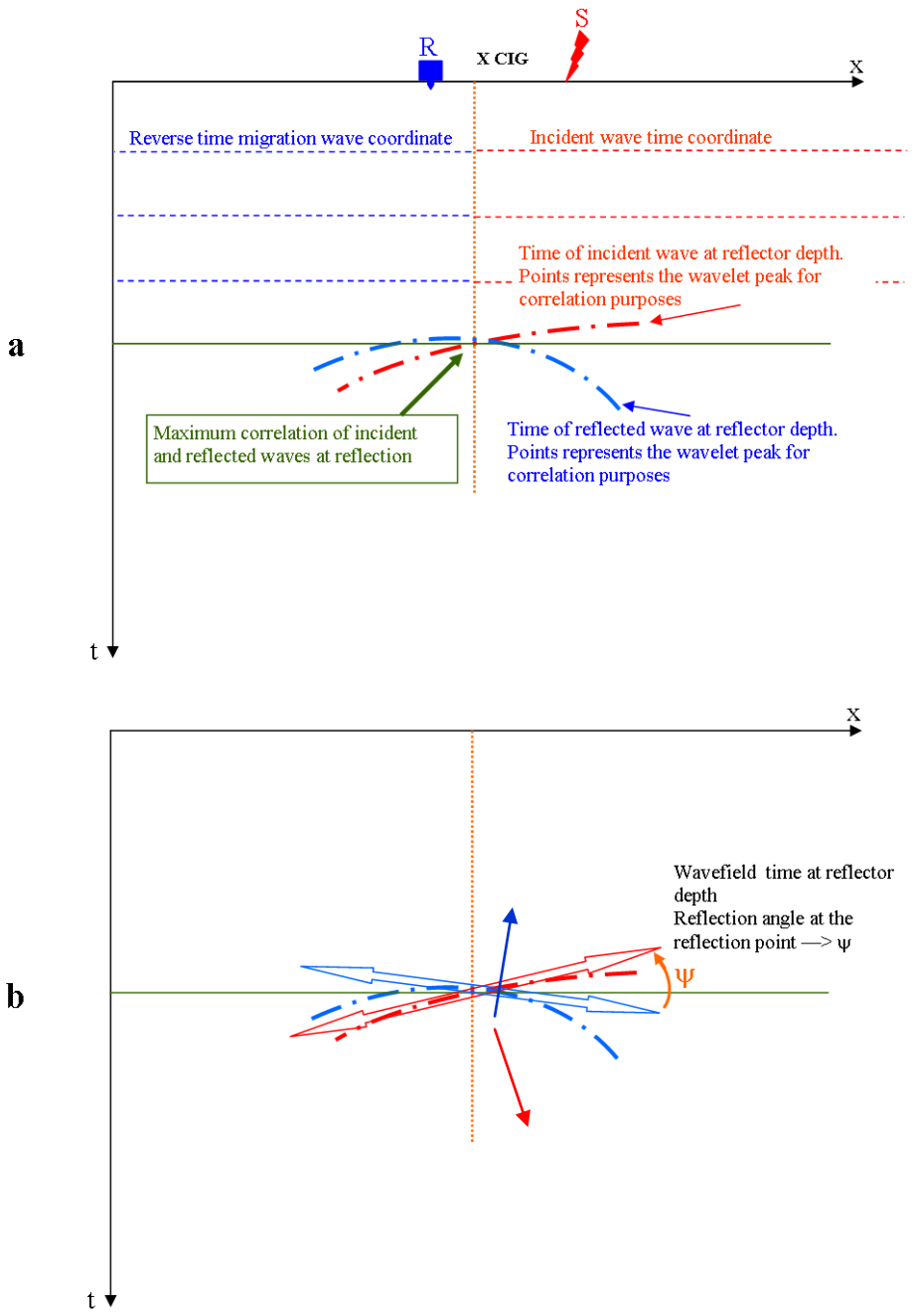

Fig. 6b The angle ψ is the reflection angle, it will be related to the gradient dz/dh on the extended imaging conditions in the depth domain (Part. 2)

The slope of the downgoing wavefield (red arrow) is a measure of its ray parameter. Knowing the velocity model the ray parameter at the surface can be related to the angle of incidence.
The slope of the upgoing wavefield (blu arrow) is a measure of its ray parameter. Knowing the velocity model, the ray parameter at the surface and reverse time backpropagating the wavefield, this can be related to the angle of reflection.
Correlation of downgoing and upgoing wavefields will be maximal at the reflection point and theoretically will continue upward for horizontal reflectors and homogeneous , isotropic formations.
This will continue for symmetrical lateral offsets at equal distance from the X_{CIG} position –h/2. +h/2.
Fig. 7 is the schematic representation (E. Robein 2010) of the correlation points at constant time Intervals.
For dipping reflectors however the maximal correlation at the reflecting point will not be maintained, In this case the schematic of Fig. 5 is introduced , where the correlation function is related to the reflection angle.

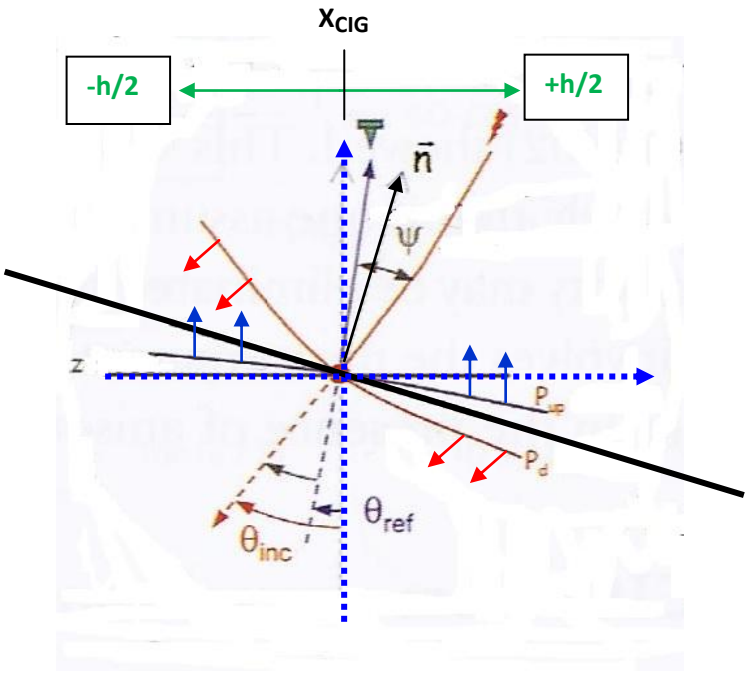

Fig. 7 Relationship between scattering angle and Incident and reflected wavefront at depth z.
Cy: E. Robein

End of part 1.

A. Piasentin
GeoNeurale Research

GeoNeurale
Am Nymphenbad 8
81245 München
research@GeoNeurale.com
www.GeoNeurale.com

T +49 (0)89 89691118
F +49 (0)89 89691117